Supplementary Material (ESI) for ***CrystEngComm 2020***.

Five water-stable luminescent Cd^{II}-based metal-organic frameworks as sensors for highly sensitive and selective detection of acetylacetone, Fe^{3+} and $Cr_2O_7^{2-}$ ions

Yong-Sheng Shi[a], Dong Liu[a], Lianshe Fu[b], Yue-Hua Li[a], Gui-Ying Dong[a]*

[a]*College of Chemical Engineering, Hebei Key Laboratory for Environment Photocatalytic and Electrocatalytic Materials, North China University of Science and Technology, No. 21 Bohai Road, Caofeidian new-city, Tangshan, Hebei, 063210, P. R. China*

[b]*Department of Physics and CICECO-Aveiro Institute of Materials, University of Aveiro, 3810-193 Aveiro, Portugal*

*Corresponding author: Gui-Ying Dong

Fax: +86-0315-8805462. Tel: +86-0315-8805460

E-mail: tsdgying@126.com.

Table Titles:

Table S1a Crystal data and structure refinements for the **1**−**3**

Cd-MOFs	**1**	**2**	**3**
Chemical formula	$C_{26}H_{20}CdCl_2N_4O_4$	$C_{54}H_{44}Cd_2Cl_4N_8O_8$	$C_{45}H_{34.5}Cd_2Cl_4N_6O_{10.25}$
Formula weight	635.76	1299.57	1216.94
Crystal system	monoclinic	Monoclinic	Monoclinic
Space group	$P2_1/n$	P_2/n	$P2_1/n$
a (Å)	9.304(2)	14.993(3)	18.478(4)
b (Å)	15.944(3)	21.331(4)	9.489(2)
c (Å)	17.445(4)	16553(2)	26.833(4)
α (°)	90	90	90
β (°)	94.552(2)	98.640(2)	91.811(2)
γ (°)	90	90	90
V (Å^3)	2579.84(11)	5224.19(16)	4702.54(16)
Z	4	4	4
D_{calcd} (g/cm^3)	1.637	1.652	1.719
Absorption coefficient, mm^{-1}	1.094	1.082	1.196
F(000)	1272	2608	2370
Crystal size, mm	0.27 x 0.26 x 0.23	0.24 x 0.22 x 0.20	0.26 x 0.22 x 0.21
θ range, deg	4.684 – 61.052	4.412 – 61.112	4.41 – 61.152
Index range h, k, l	-13/11, -22/22, -24/23	-21/21, -30/29, -15/23	-25/25, -12/13, -36/35
Reflections collected	37137	77199	70559
Independent reflections (R_{int})	7603 (0.0380)	15324 (0.0595)	13816 (0.0376)
Data/restraint/parameters	7603/0/334	15324/0/687	13816/82/623
Goodness-of-fit on F^2	1.023	1.031	0.989
Final R_1, wR_2 ($I > 2\sigma(I)$)	0.0300, 0.0690	0.0472, 0.1192	0.0363, 0.0796
Largest diff. peak and hole	0.68, -0.66	2.11, -1.39	1.17, -0.96

Table S1b Crystal data and structure refinements for the **4** and **5**

Cd-MOFs	**4**	**5**
Chemical formula	$C_{38}H_{30}CdCl_2N_6O_4$	$C_{20}H_{17}Cd_{0.5}ClN_3O_2$
Formula weight	870.33	423.02
Crystal system	Triclinic	monoclinic
Space group	$P\bar{1}$	$C2/c$
a (Å)	9.628(6)	13.1061(5)
b (Å)	10.279(4)	16.0142(5)
c (Å)	18.731(9)	17.5495(7)
α (°)	91.228(4)	90
β (°)	101.525(4)	97.736(4)
γ (°)	90.458(4)	90
V (Å^3)	1815.83(16)	1051.6(2)
Z	2	8
D_{calcd} (g/cm^3)	1.564	1.540
Absorption coefficient, mm^{-1}	0.805	0.796
F(000)	870	1720
Crystal size, mm	0.26 x 0.23 x 0.22	0.20 x 0.16 x 0.12
θ range, deg	5.326-62.064	4.452-61.162
Index range h, k, l	-13/13, -14/14, -26/26	-18/18, -22/22, -24/24
Reflections collected	42306	26620
Independent reflections (R_{int})	9988(0.0763)	5301 (0.0524)
Data/restraint/parameters	9988 / 0 / 460	5301 / 639 / 240
Goodness-of-fit on F^2	1.036	1.048
Final R_1, wR_2 ($I > 2\sigma(I)$)	0.0735, 0.1846	0.0458, 0.1295
Largest diff. peak and hole	2.31, -0.89	0.85, -1.13

Table S2a Selected Bond Lengths [Å] and Angles [º] for the **1** and **2**

Parameter	Value	Parameter	Value
1			
Cd1–O1/O2	2.201(2)	Cd1–N1	2.236(2)
Cd1–O3B/O4B	2.227(2)	Cd1–N4A	2.249(2)
O1–Cd1–O4B	121.17(7)	O1–Cd1–N1	121.27(6)
O1–Cd1–N4A	99.10(6)	O4B–Cd1–N1	94.50(6)
O4B–Cd1–N4A	111.32(7)	N1–Cd1–N4A	109.72(7)
2			
Cd1–O1/O1A	2.249(2)	Cd1–O2/O2A	2.615(2)
Cd1–N1/N1A	2.099(2)	Cd2–O5/O5D	2.174(2)
Cd2–N3/N3D	2.221(3)	Cd3–O7/O7F	2.175(2)
Cd3–N5/N5F	2.210(3)	Cd4–O4B/O4C	2.407(2)
Cd4–O3B/O3C	2.341(2)	Cd4–N8/N8G	2.239(2)
O4B–Cd4–O4C	128.09(11)	N8–Cd4–O4B	99.64(9)
O3C–Cd4–O4C	55.34(8)	N8–Cd4–O4C	114.79(8)
O3B–Cd4–O4B	55.34(8)	N8–Cd4–O3B	168.92(9)
O3C–Cd4–O4B	85.06(8)	N8G–Cd4–O3C	91.23(9)
O3B–Cd4–O4C	85.06(8)	N8–Cd4–O3B	91.23(9)
O3B–Cd4–O3C	83.16(12)	N8G–Cd4–O3B	168.92(9)
N8G–Cd4–O4B	114.79(8)	N8G–Cd4–N8	95.81(13)
N8G–Cd4–O4C	99.64(9)	O1–Cd1–N1A	116.89(8)
O1A–Cd1–O1	122.62(12)	O1–Cd1–N1	100.00(8)
O1–Cd1–O2	53.12(7)	O2–Cd1–O2A	82.68(11)
O1A–Cd1–O2A	53.12(7)	N1–Cd1–O2A	94.99(8)
O1A–Cd1–O2	83.06(8)	N1A–Cd1–O2A	153.13(8)
O1–Cd1–O2A	83.06(8)	N1A–Cd1–O2	94.98(8)
O1A–Cd1–N1	116.89(8)	N1–Cd1–O2	153.13(8)
O1A–Cd1–N1A	100.00(8)	N1–Cd1–N1A	98.63(13)
O7F–Cd3–O7	102.13(12)	O5–Cd2–O5D	107.25(12)
O7–Cd3–N5F	118.60(9)	O5–Cd2–N3D	119.32(10)
O7F–Cd3–N5F	105.67(9)	O5D–Cd2–N3D	102.00(9)
O7F–Cd3–N5	118.60(9)	O5–Cd2–N3	101.99(9)
O7–Cd3–N5	105.67(9)	O5D–Cd2–N3	119.32(10)
N5–Cd3–N5F	106.88(14)	N3D–Cd2–N3	107.95(15)

symmetry code: A: –*x*, 1–*y*, 1–*z*, B: 0.5–*x*, –0.5+*y*, 0.5–*z* for **1**; A: 0.5–*x*, *y*, 0.5–*z*; B: 1-*x*, –*y*, 1–*z*; C: 0.5+*x*, –*y*, 1.5+*z*, D: 0.5–*x*, *y*, 1.5–*z*; F: 0.5–*x*, *y*, 2.5–*z*, G: 1.5–*x*, *y*, 2.5–*z* for **2**.

Table S2b Selected bond lengths [Å] and angles [°] for Cd-MOFs **3**–**4**.

Parameter	Value	Parameter	Value
3			
Cd1–O1	2.265(2)	Cd1–N6B	2.392(2)
Cd1–O2	2.629(2)	Cd2–N2	2.275(2)
Cd1–O3	2.328(2)	Cd2–O5	2.275(4)
Cd1–O4	2.5263(2)	Cd2–O6	2.581(5)
Cd1–O4A	2.4207(2)	Cd2–O7C	2.361(4)
Cd1–N1	2.324(2)	Cd2–O8C	2.420(5)
Cd2–N4	2.233(2)	O4A–Cd1–O4	68.47(7)
O1–Cd1–O2	52.49(8)	N1–Cd1–O2	89.64(7)
O1–Cd1–O3	126.49(9)	N1–Cd1–O3	94.20(8)
O1–Cd1–O4	82.31(8)	N1–Cd1–O4A	80.81(7)
O1–Cd1–O4A	88.60(8)	N1–Cd1–O4	128.04(7)
O1–Cd1–N1	139.18(9)	N1–Cd1–N6B	94.81(9)
O1–Cd1–N6B	93.54(9)	N6B–Cd1–O2	80.96(8)
O3–Cd1–O2	163.73(8)	N4–Cd2–O7C	98.68(12)
O3–Cd1–O4	53.38(7)	N4–Cd2–O8C	130.47(18)
O3–Cd1–O4A	99.20(8)	O5–Cd2–O6	51.45(12)
O3–Cd1–N6B	82.96(9)	O5–Cd2–O7C	83.87(17)
N2–Cd2–O5	106.83(16)	O5–Cd2–O8C	91.41(19)
N2–Cd2–O6	101.8(2)	O7C–Cd2–O6	115.9(2)
N2–Cd2–O7C	137.37(11)	O7C–Cd2–O8C	53.56(11)
N2–Cd2–O8C	84.49(10)	O8C–Cd2–O6	142.7(2)
N4–Cd2–N2	104.55(8)	N4–Cd2–O6	83.96(13)
N4–Cd2–O5	129.38(13)		
4			
Cd1–O2	2.398(4)	Cd1–N3C	2.383(4)
Cd1–N1	2.327(4)	Cd1–N6D	2.368(4)
Cd1–O1	2.413(4)	Cd1–O3	2.233(5)
O2–Cd1–O1	54.44(14)	N6D–Cd1–O1	87.55(16)
N1–Cd1–O2	146.49(14)	N6D–Cd1–N3C	169.98(15)
N1–Cd1–O1	93.46(14)	O3–Cd1–O2	114.9(2)
N1–Cd1–N3C	87.02(15)	O3–Cd1–N1	97.8(2)
N1–Cd1–N6D	90.66(16)	O3–Cd1–O1	168.5(2)
N3C–Cd1–O2	80.24(15)	O3–Cd1–N3C	100.0(2)
N3C–Cd1–O1	82.87(15)	O3–Cd1–N6D	90.0(2)
N6D–Cd1–O2	96.56(16)		

symmetry code: A: -*x*, 2-*y*, 1-*z*, B: 1–*x*, 2–*y*, 1–*z*, C: 0.5+*x*, 0.5–*y*, 0.5+*z* for **3**; C:1+*x*, *y*, *z*; D: *x*, 1+*y*, *z*. for **4.**

Table S2c Selected bond lengths [Å] and angles [°] for Cd-MOFs **5**.

Parameter	Value	Parameter	Value
5			
Cd1–N1/N1A	2.283(2)	Cd1–O1/O1A	2.382(2)
Cd1–O2/O2A	2.382(2)	N11–Cd1–O2A	133.14(12)
N1A–Cd1–N1	89.91(13)	N1–Cd1–O2A	93.91(10)
N1–Cd1–O1A	135.46(12)	O1A–Cd1–O1	114.2(2)
N1A–Cd1–O1	135.46(12)	O2A–Cd1–O1A	53.56(11)
N11–Cd1–O1A	93.20(10)	O2–Cd1–O1	53.56(10)
N1–Cd1–O1	93.20(10)	O2–Cd1–O1A	90.98(15)
N1–Cd1–O2	133.14(12)	O2A–Cd1–O1	90.98(15)
N1A–Cd1–O2	93.91(10)	O2–Cd1–O2A	115.8(2)

symmetry code: A:1–*x*, *y*, 1.5–*z* for **5**.

Table S3 Hydrogen bonds (Å) and angles (˚) for the **1**/**2**

Donor–H···acceptor	D–H	H···A	D···A	Angle
1				
N2C–H2C ···O3C	0.86	1.94	2.743(3)	156
N3C–H3C ···O2C	0.86	1.98	2.770(3)	153
2				
N2H–H3H ···O3H	0.86	1.89	2.735(3)	167
N4I–H3I ···O2I	0.86	1.96	2.758(4)	154
N6J–H6J ···O6J	0.86	1.95	2.745(4)	153
N7J–H7J ···O8J	0.86	2.04	2.853(3)	156

Symmetry codes for **1**: C = 1-*x*, 1-*y*, 1-*z*; Symmetry codes for **2**: H = -*x*-, -*y*, -*z*; I = 0.5+*x*, -*y*, 0.5+*z*; J = 1-*x*, 1-*y*, 2-*z*.

Table S4. Comparison of the sensitivities of **1** and **2** for acac with related MOFs

MOFs	LOD/M	Ref
$\{[(CH_3)_2NH_2][Zn(FDA)(BTZ)_2]\}_n$	6.47×10^{-7}	[9]
$\{[Zn_3(bbib)_2(ndc)_3]\cdot2DMF\cdot2H_2O\}_n$	0.10×10^{-7}	[5]
$\{[Co_{1.5}(TBIP)_{1.5}(L)]\cdot0.5H_2O\}_n$	0.023×10^{-6}	[6]
2	6.36×10^{-7}	This work
3	8.76×10^{-7}	This work

H_2FDA = furan-2,5-dicarboxylic acid, HBTZ = 1*H*-benzotriazole, bbib = 1,3-bis(benzimidazolyl)benzene, H_2ndc = 1,4-naphthalenedicarboxylic acid, L = 1,3-bis(5,6-dimethylbenzimidazol-1-yl)propane, and H_2TBIP = 5-tert-butylisophthalic acid.

Table S5. Comparison of the sensitivities of **2** with previously reported MOFs to Fe^{3+} ions

MOFs	LOD/M	Ref
$\{[Zn(bbib)(oba)]\cdot solvents\}_n$	3.31×10^{-6}	[2]
$[Zn_5(hfipbb)_4(trz)_2(H_2O)_2]_n$	0.2×10^{-3}	[11]
$[Zn_2L_2]\cdot2DMF\cdot2MeOH$	0.1×10^{-3}	[1]
2	6.42×10^{-5} M	This work

bbib = 1,3-bis(benzimidazolyl)benzene, oba = 4,4'-oxybisbenzoate; H_2hfipbb = 4,4,(hexafluoroisopropylidene)bis(benzoic acid), Htrz = 1H-1,2,3-triazole; H_2L= 8-hydroxyquinolinate derivative.

Table S6. Comparison of the sensitivities of **3** with previously reported MOFs to $Cr_2O_7^{2-}$ ions

MOFs	LOD/M	Ref
$\{[Co_{1.5}(TBIP)_{1.5}(L)]\cdot 0.5H_2O\}_n$	2.09×10^{-4}	[6]
$\{[Cd_2(L)(DMA)]\cdot[H_2N(Me)_2]\}_n$	2.54×10^{-3}	[4]
$Zr_6O_4(OH)_7(H_2O)_3(BTBA)_3$	1.5×10^{-6}	[8]
2	1.99×10^{-5} M	This work

L = 1,3-bis(5,6-dimethylbenzimidazol-1-yl)propane, and H_2TBIP = 5-tert-butylisophthalic acid; H_5L= 2,4-di(3,5dicarboxylphenyl)benzoic acid; H_3BTBA=4,4′,4″-(1Hbenzo[d]imidazole-2,4,7-triyl)tribenzoic acid.

Fig. S1. (a) The $DCTP^{2-}$ anions create a 1D infinite $[Cd(DCTP)]_n$ chain by linking adjacent Cd^{II} ions in **1**; the binuclear $[Cd_2(L)_2]$ unit was formed by L1 ligands and Cd^{II} atoms; (c) the 3D supramolecular network of **1** formed by two hydrogen bonds interactions (Pink dotted line).

Fig. S2. (a) two varying 1D chains, named as $[(Cd1)(Cd2)(L2)]_n$, $[(Cd3)(Cd4)(L2)_2]_n$ were formed by L2 ligands and Cd^{II} atoms in **2**; (b) Two 1D "V" like chains($[(Cd1)(Cd4)(DCTP)]_n$ and $[(Cd2)(Cd3)(DCTP]_n$) with the surrounding Cd^{II} centers in **2** (c) the 3D supramolecular network of **2** formed by two hydrogen bonds interactions (pink dotted line).

Fig. S3. (a) The $DCTP^{2-}$ anions connect the adjacent Cd^{II} ions using these two coordination modes in **3;** (b) The μ_3-bridging L3 ligands adopt the *cis*-conformation to form a rhombus unit $[Cd_4(L3)_2]$ in **3.** (c) 3,3,4,5-connected topology of **3** (the green, blue and red nodes represent Cd^{II} center, L3 ligands and $DCTP^{2-}$ anions, respectively).

Fig. S4. (a) Two different $DCTP^{2-}$ anions link adjacent Cd^{II} atoms to form a 1D infinite chain $[Cd(DCTP)]_n$ in **4**; (b) 2D network $[Cd(L4)]_n$ is formed by using μ_3-bridging L4 ligands with a *cis*-conformation fashion to connect Cd^{II} ions; (c) an rarely 2-nodal (3,5)-connected **gra** topological network of **4** (the green and blue represent Cd^{II} center and L3 ligands, respectively).

Fig. S5. (a) 1D"V" like chains, named as **1D** $[Cd(L5)]_n$ is formed by L5 ligands and Cd^{II} atoms in **5**; (b) 1D "V" like chains$[Cd(DCTP)]_n$ is formed by $DCTP^{2-}$ ligands and Cd^{II} atoms in **5.**

Fig. S6. The infrared spectrum of Cd-MOFs **1**–**5.**

Fig. S7. The PXRD pattern of the bulk sample is consistent with the simulated pattern of the single crystal structure in Cd-MOFs **1**–**5.**

Fig. S8. Soild luminescence lifetime of Cd-MOFs **1**–**5.**

Fig. S9. Time-dependent emission spectra of **2** (a) and **3** (b) suspended in aqueous solutions.

Fig. S10. PXRD patterns of **2** and **3** under simulated conditions.

Fig. S11. The change of the fluorescence emission intensity of **2** (a) and **3** (b) in different pH solutions.

Fig. S12. The PXRD patterns of **2** (a) and **3** (b) were measured in different solvents.

Fig. S13. Spectral overlap between the absorption spectra of acac ions and the excitation spectra of **2** and **3**.

Fig. S14. In **2**, the time required for the quenching efficiency of Fe^{3+} ions to reach the maximum.

Fig. S15. The PXRD patterns of **2** sample was immersed in EtOH/H_2O solution containing Fe^{3+} ions and other common cations.

Fig. S16. Spectral overlap between the absorption spectra of Fe^{3+} ions and the excitation spectra of **2**.

Fig. S17. In **3**, the time required for the quenching efficiency of $Cr_2O_7^{2-}$ anions to reach the maximum.

Fig. S18. The PXRD patterns of **3** sample was immersed in EtOH/H_2O solution containing $Cr_2O_7^{2-}$ anions and other common anions.

Fig. S19. Spectral overlap between the absorption spectra of $Cr_2O_7^{2-}$ anions and the excitation spectra of **3**.

Fig. S20. TGA curves of Cd-MOFs **1**–**5.**

Fig. S21. Comparison of the quenching efficiency of **2** for sensing acac/Fe^{3+}, and **3** for acac/$Cr_2O_7^{2-}$ over three cycles.

Fig. S22. (a) Effects of pH on the fluorescence maxima of **2** + acac (circle) and **2** + Fe^{3+} (triangle); (a) Effects of pH on the fluorescence maxima of **3** + acac (circle) and **3** + $Cr_2O_7^{2-}$ (triangle). Solvent: EtOH/H_2O (1:1, v/v).

Fig. S23. The EDX patterns of **2** and **3**; **2** + acac, **3** + acac; **2** + Fe^{3+}, **3** + $Cr_2O_7^{2-}$, respectively.

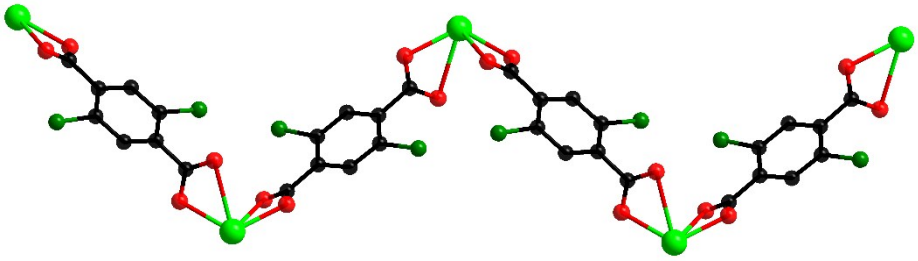

(a)

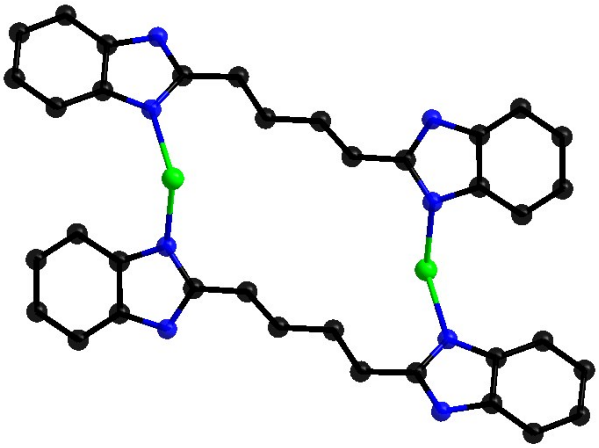

(b)

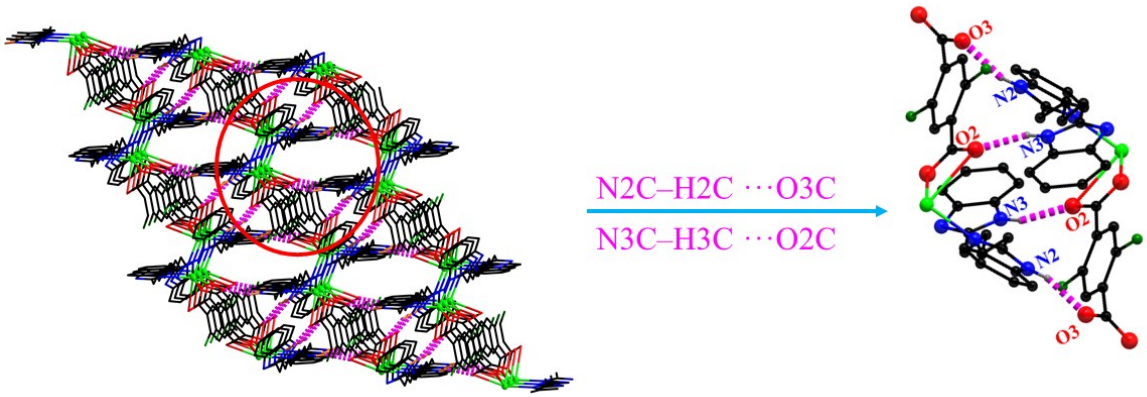

(c)

Fig. S1. (a) The $DCTP^{2-}$ anions create a 1D infinite $[Cd(DCTP)]_n$ chain by linking adjacent Cd^{II} ions in **1**; the binuclear $[Cd_2(L1)_2]$ unit was formed by L1 ligands and Cd^{II} atoms; (c) the 3D supramolecular network of **1** formed by two hydrogen bonds interactions (Pink dotted line).

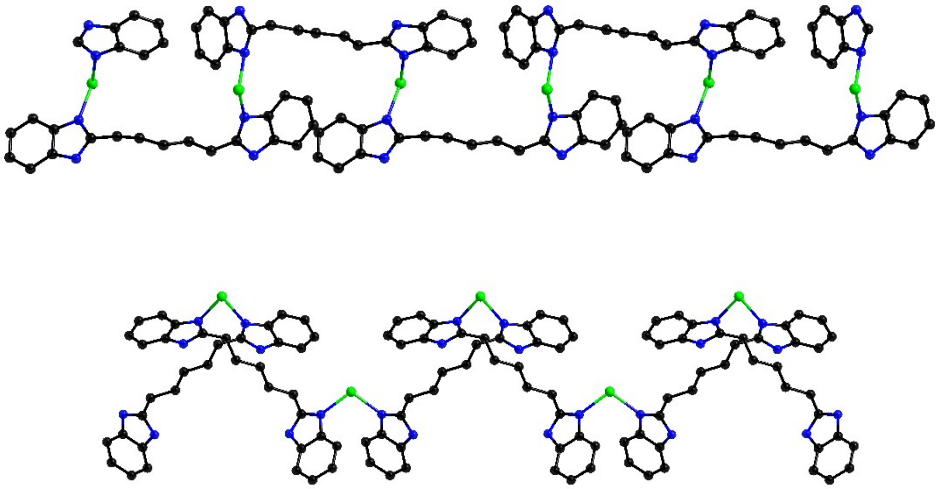

(a)

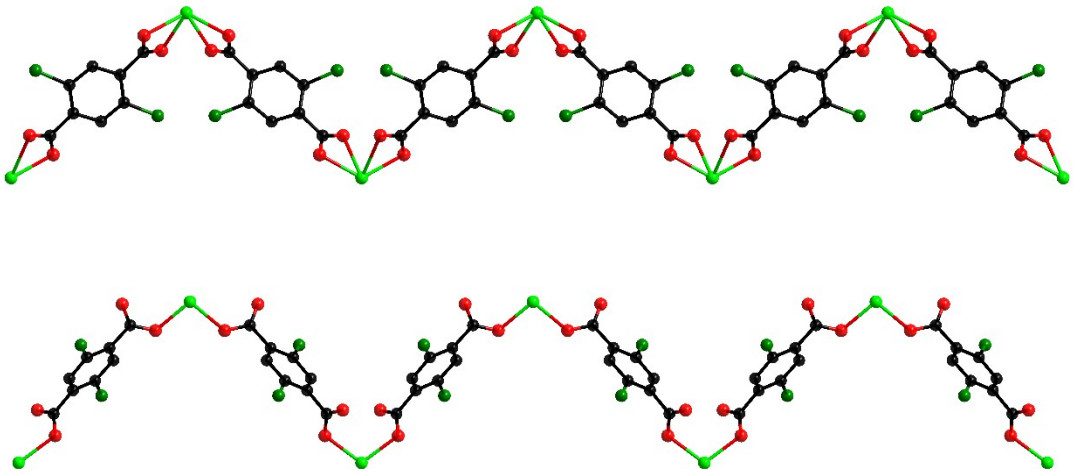

(b)

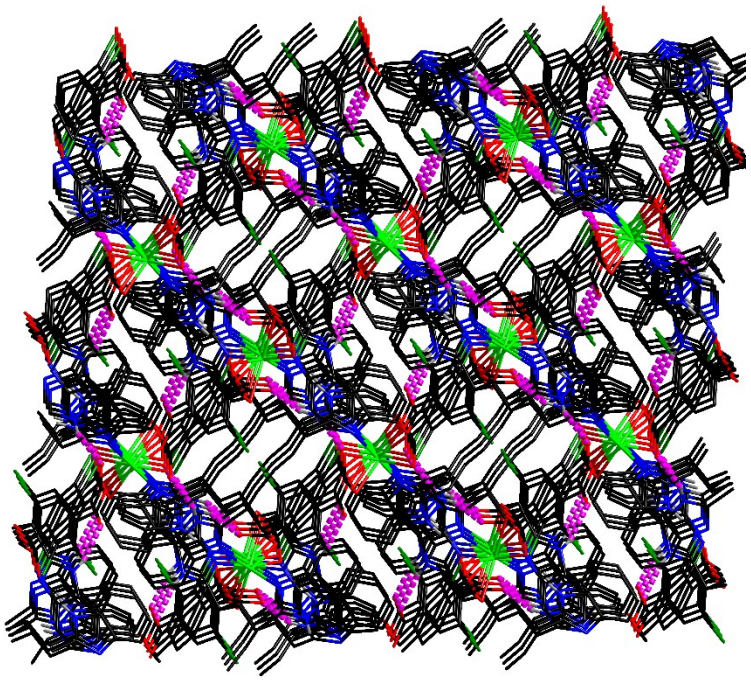

(c)

Fig. S2. (a) two varying 1D chains, named as $[(Cd1)(Cd2)(L2)]_n$, $[(Cd3)(Cd4)(L2)_2]_n$ were formed by L2 ligands and Cd^{II} atoms in **2**; (b) Two 1D "V" like chains($[(Cd1)(Cd4)(DCTP)]_n$ and $[(Cd2)(Cd3)(DCTP]_n$) with the surrounding Cd^{II} centers in **2** (c) the 3D supramolecular network of **2** formed by two hydrogen bonds interactions (pink dotted line).

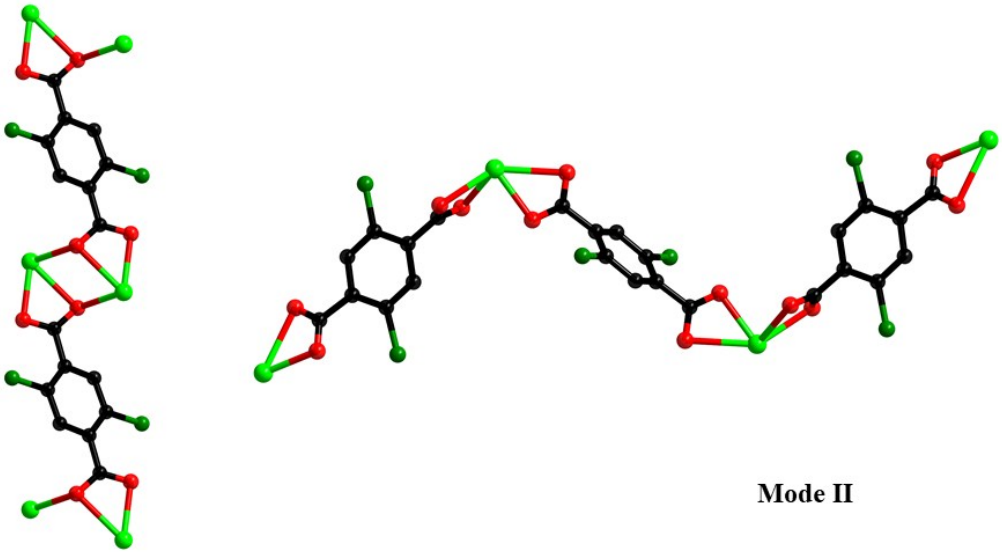

(a)

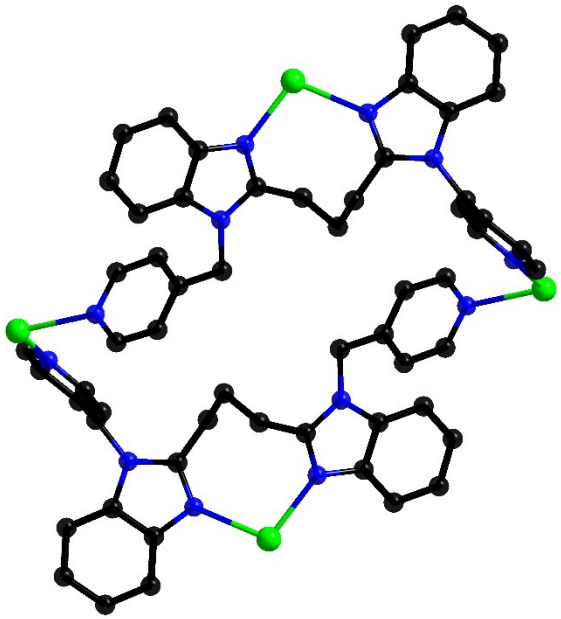

(b)

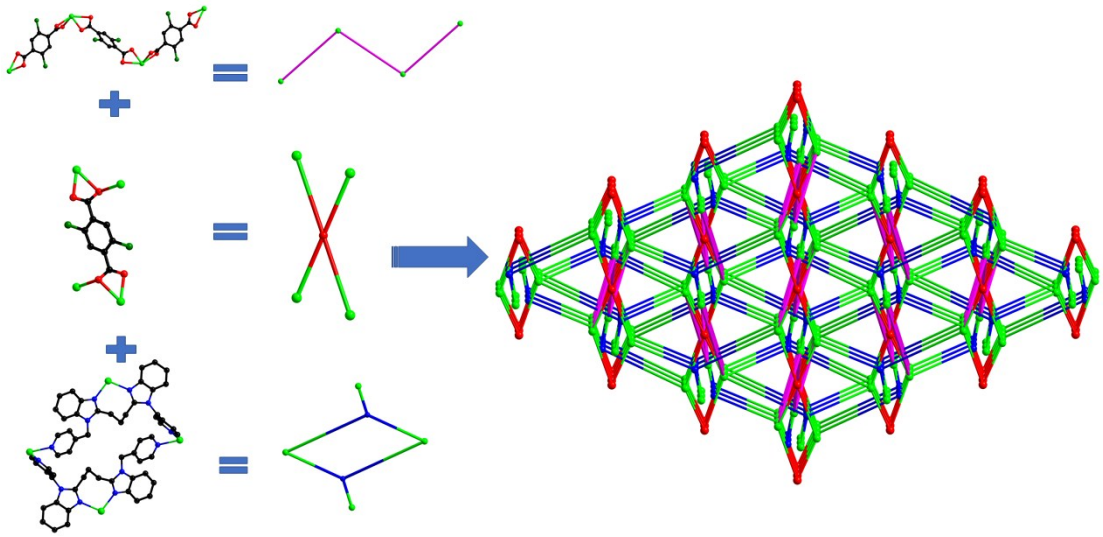

(c)

Fig. S3. (a) The $DCTP^{2-}$ anions connect the adjacent Cd^{II} ions using these two coordination modes in **3;** (b) The μ_3-bridging L3 ligands adopt the *cis*-conformation to form a rhombus unit $[Cd_4(L3)_2]$ in **3.** (c) 3,3,4,5-connected topology of **3** (the green, blue and red nodes represent Cd^{II} center, L3 ligands and $DCTP^{2-}$ anions, respectively).

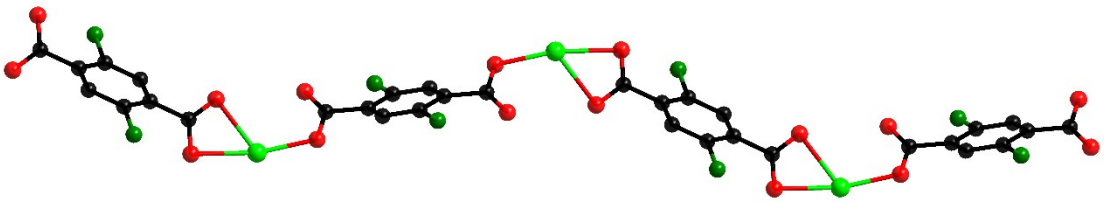

(a)

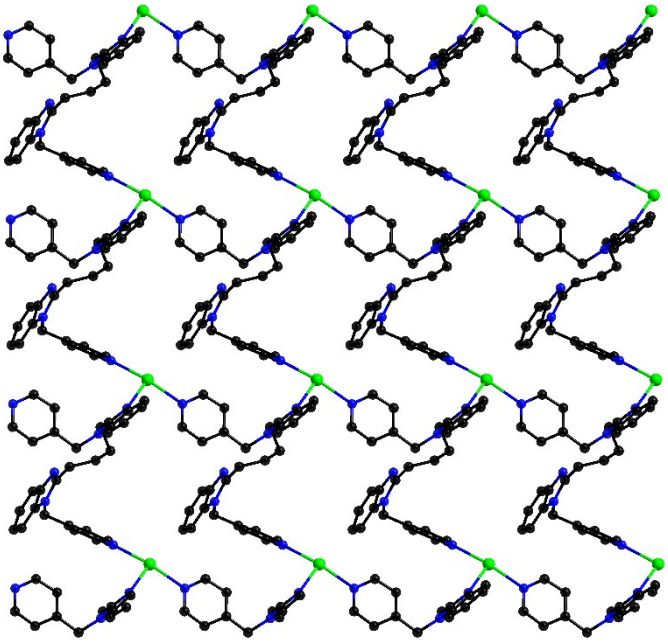

(b)

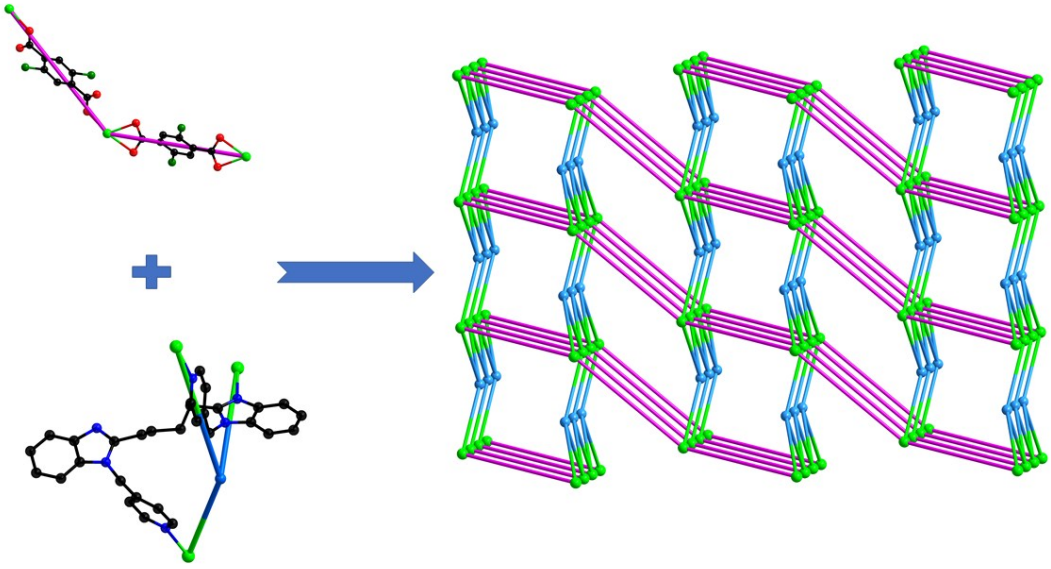

(c)

Fig. S4. (a) Two different $DCTP^{2-}$ anions link adjacent Cd^{II} atoms to form a 1D infinite chain

$[Cd(DCTP)]_n$ in **4**; (b) 2D network $[Cd(L4)]_n$ is formed by using μ_3-bridging L4 ligands with a *cis*-conformation fashion to connect Cd^{II} ions; (c) an rarely 2-nodal (3,5)-connected **gra** topological network of **4** (the green and blue represent Cd^{II} center and L3 ligands, respectively).

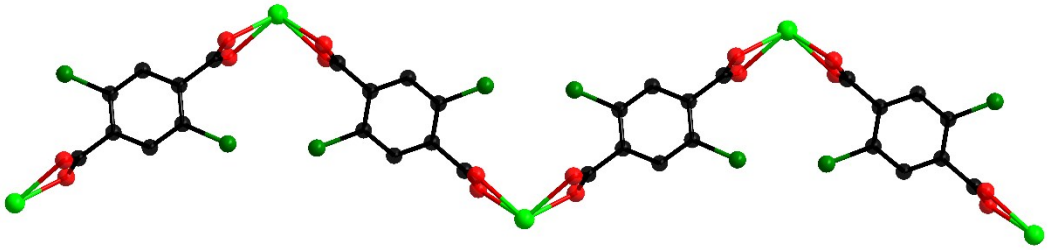

(a)

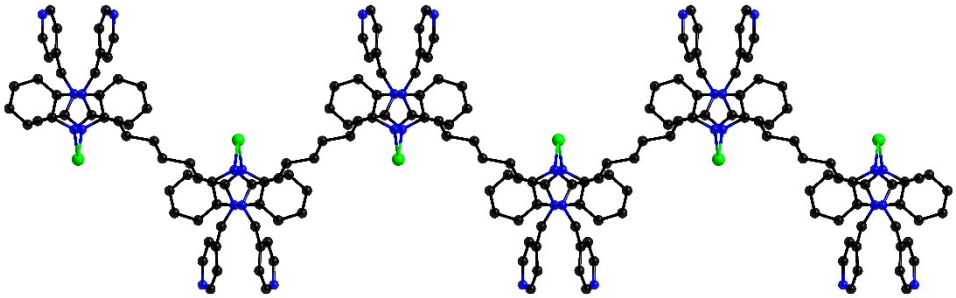

(b)

Fig. S5. (a) 1D "V" like chains, named as **1D** $[Cd(L5)]_n$ is formed by L5 ligands and Cd^{II} atoms in **5**; (b) 1D "V" like chains $[Cd(DCTP)]_n$ is formed by $DCTP^{2-}$ ligands and Cd^{II} atoms in **5.**

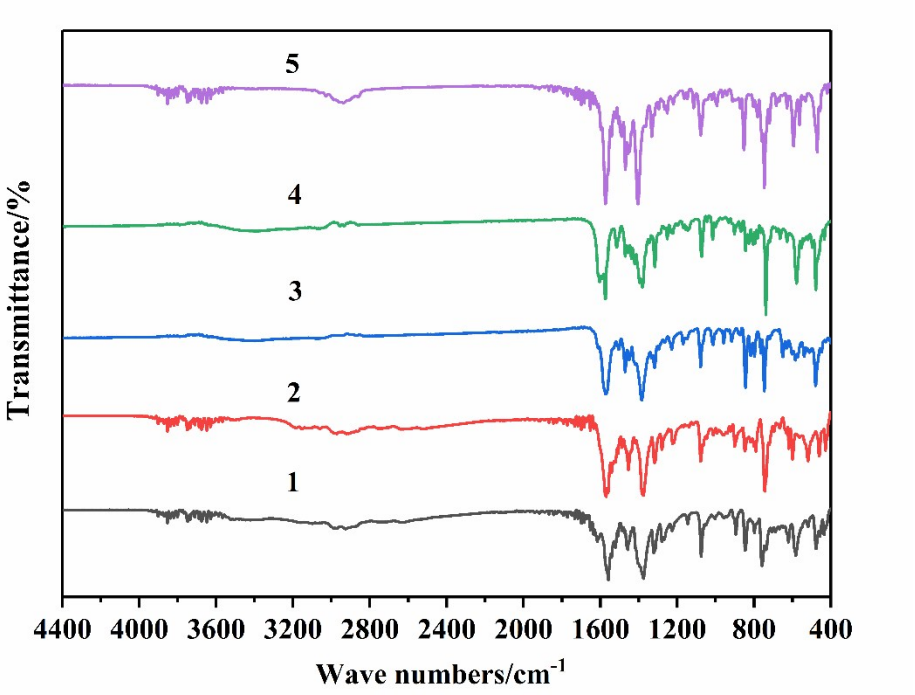

Fig. S6. The infrared spectrum of Cd-MOFs **1**–**5.**

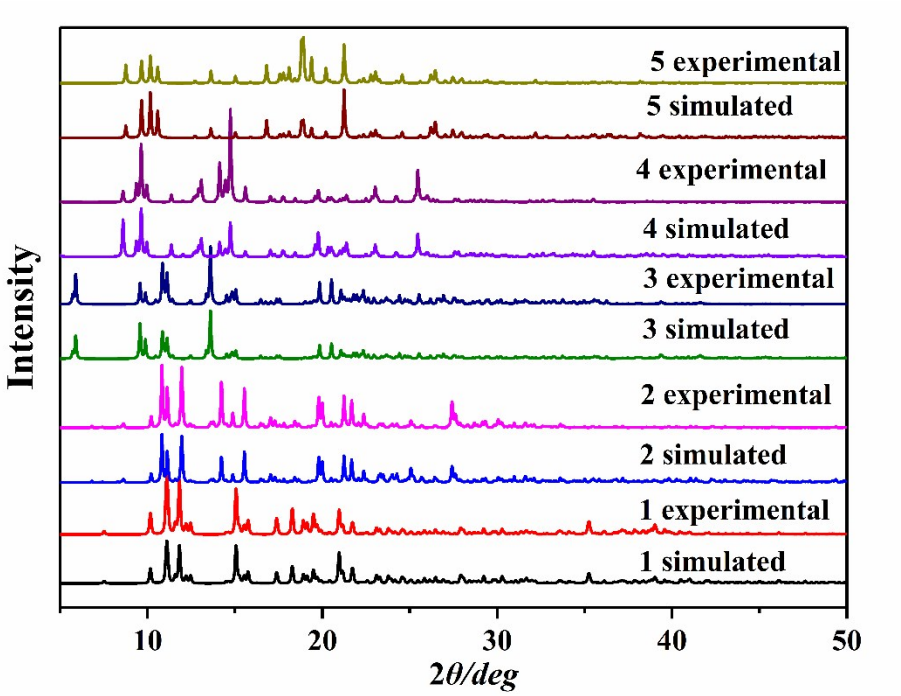

Fig. S7. The PXRD pattern of the bulk sample is consistent with the simulated pattern of the single crystal structure in Cd-MOFs **1**–**5.**

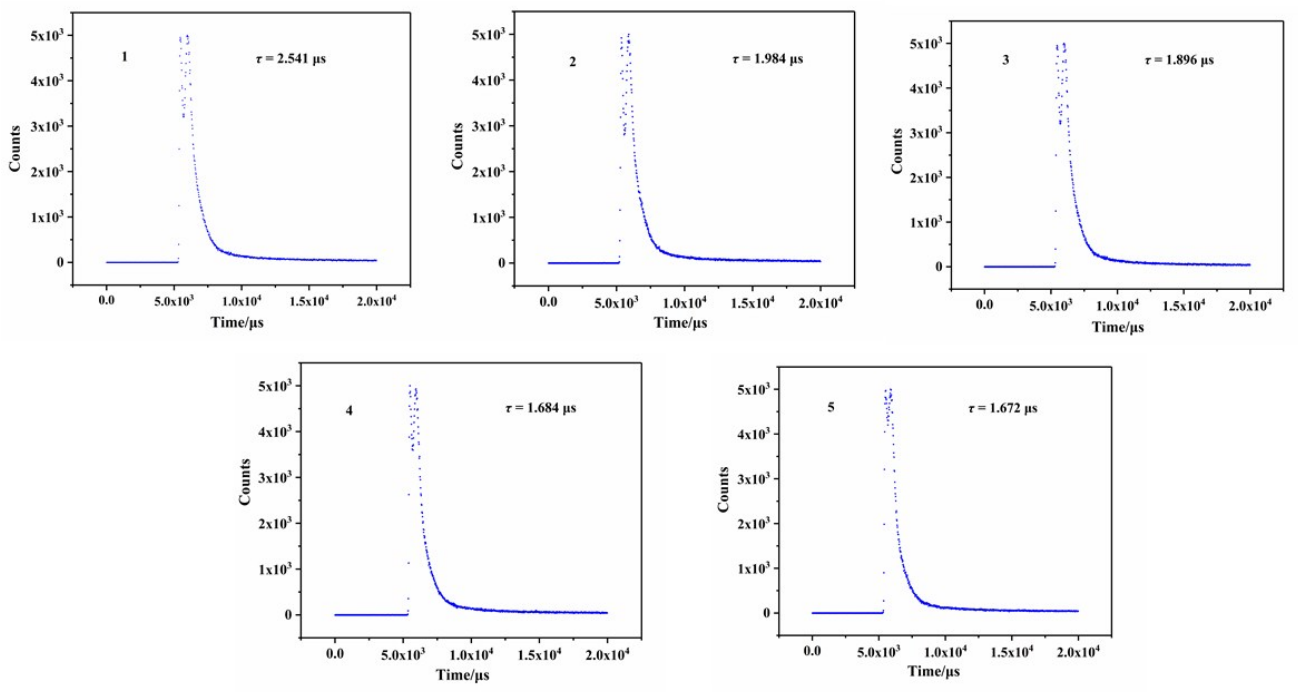

Fig. S8. Soild luminescence lifetime of Cd-MOFs **1**–**5**.

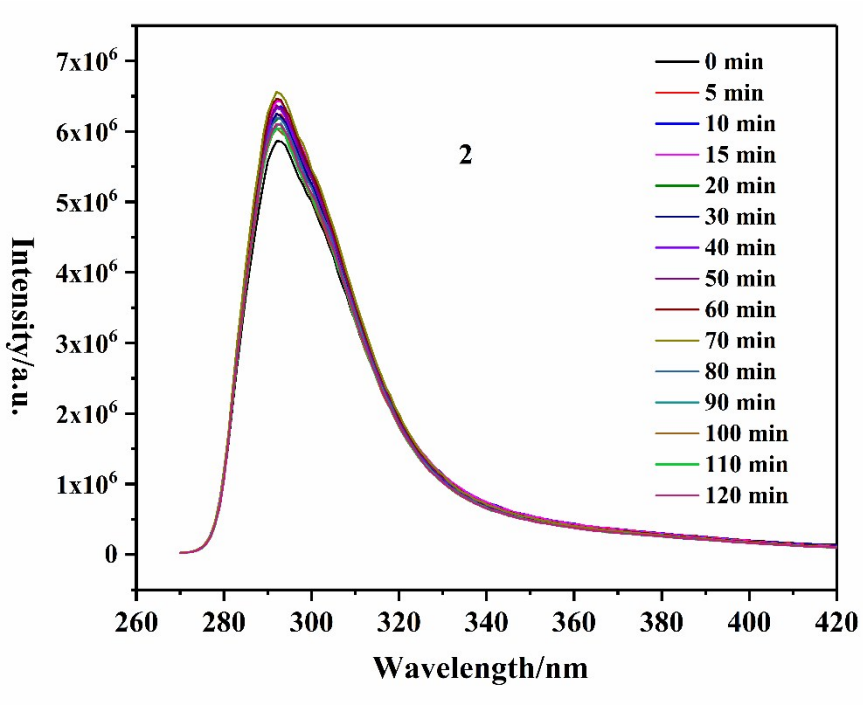

(a)

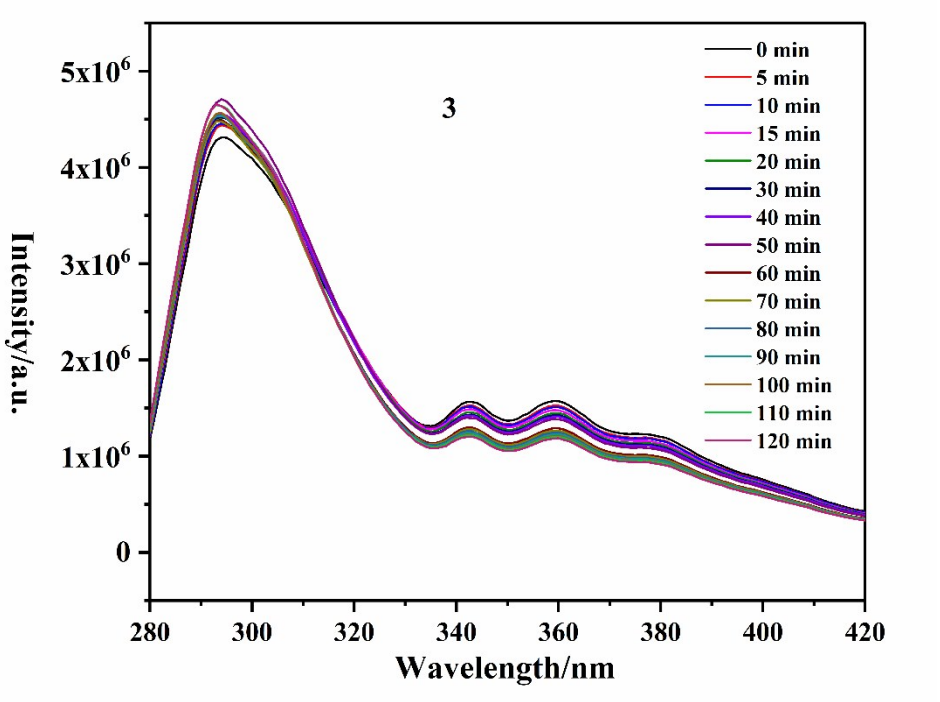

(b)

Fig. S9. Time-dependent emission spectra of **2** (a) and **3** (b) suspended in aqueous solutions.

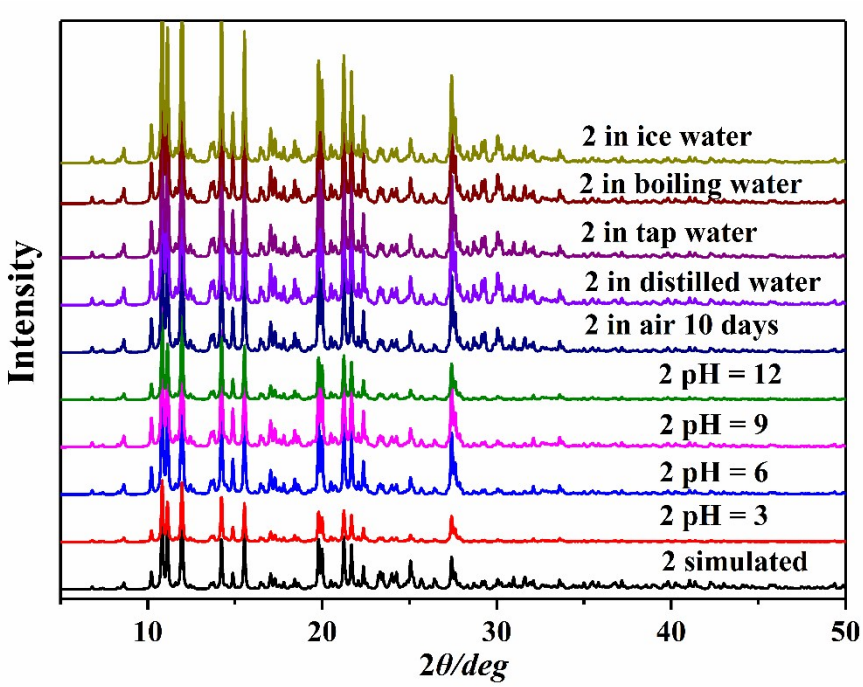

(a)

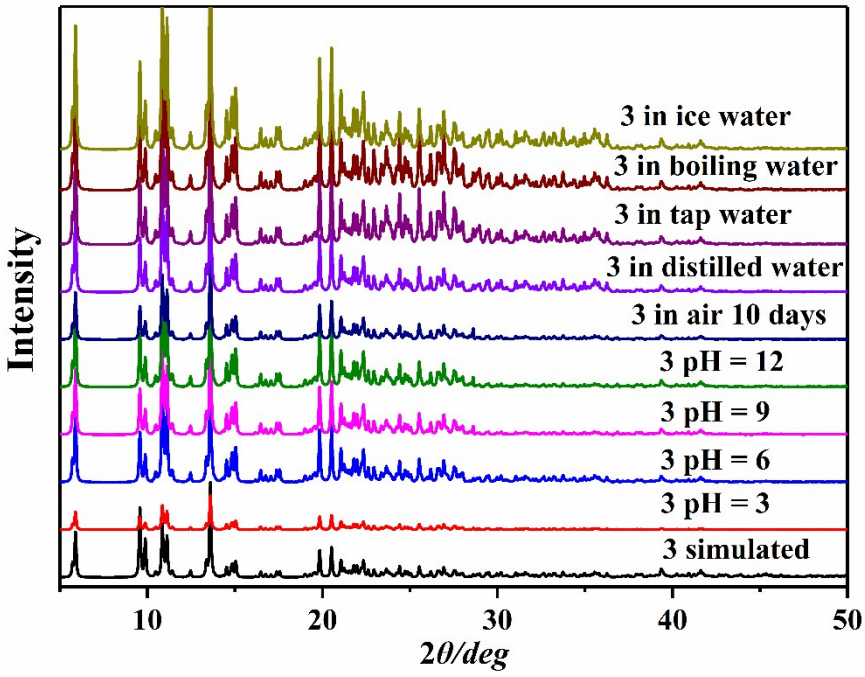

Fig. S10. PXRD patterns of **2** and **3** under simulated conditions.

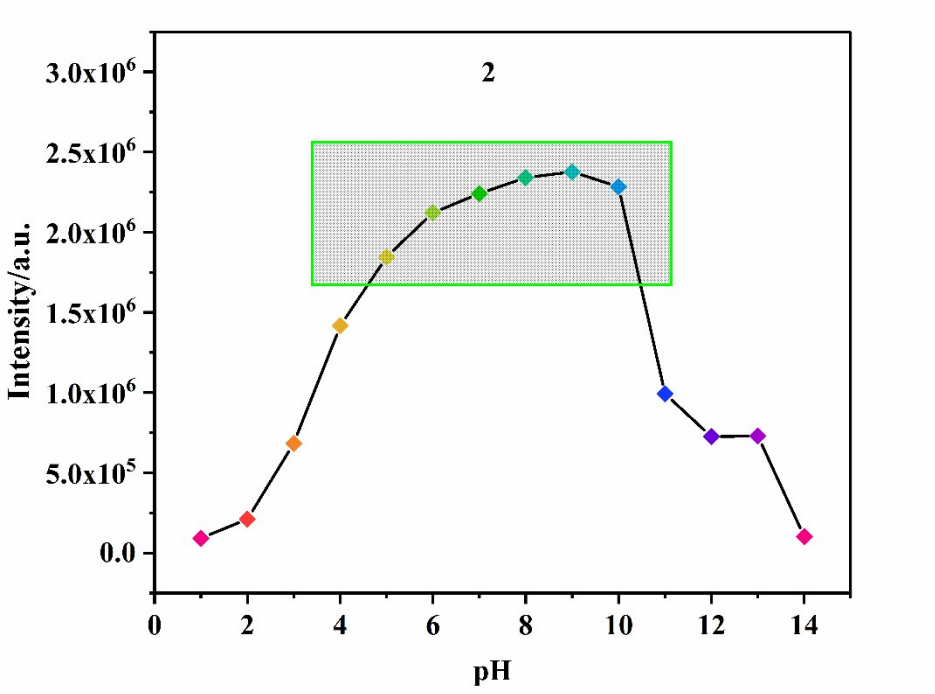

(a)

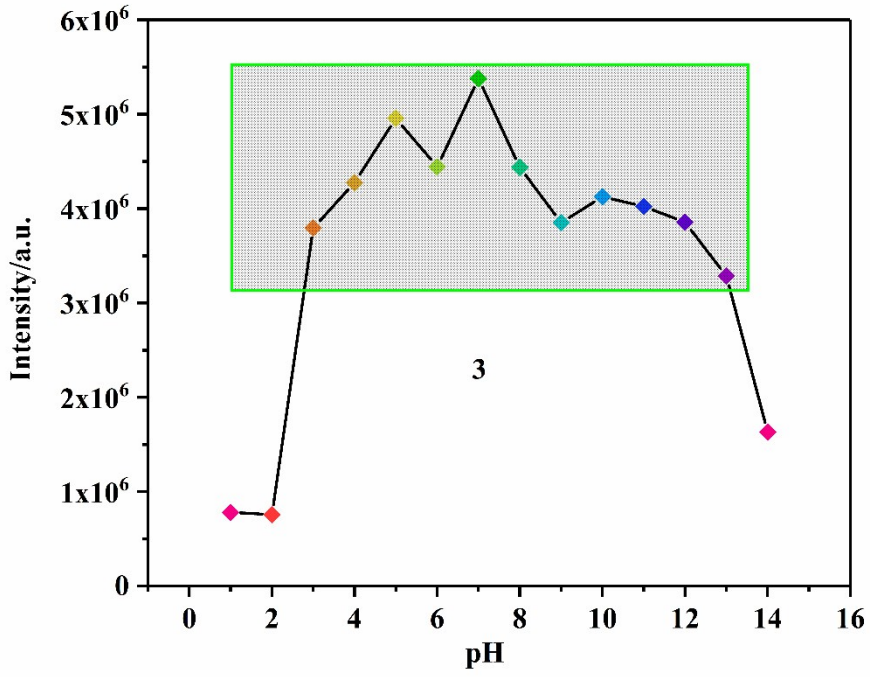

(b)

Fig. S11. The change of the fluorescence emission intensity of **2** (a) and **3** (b) in different pH solutions.

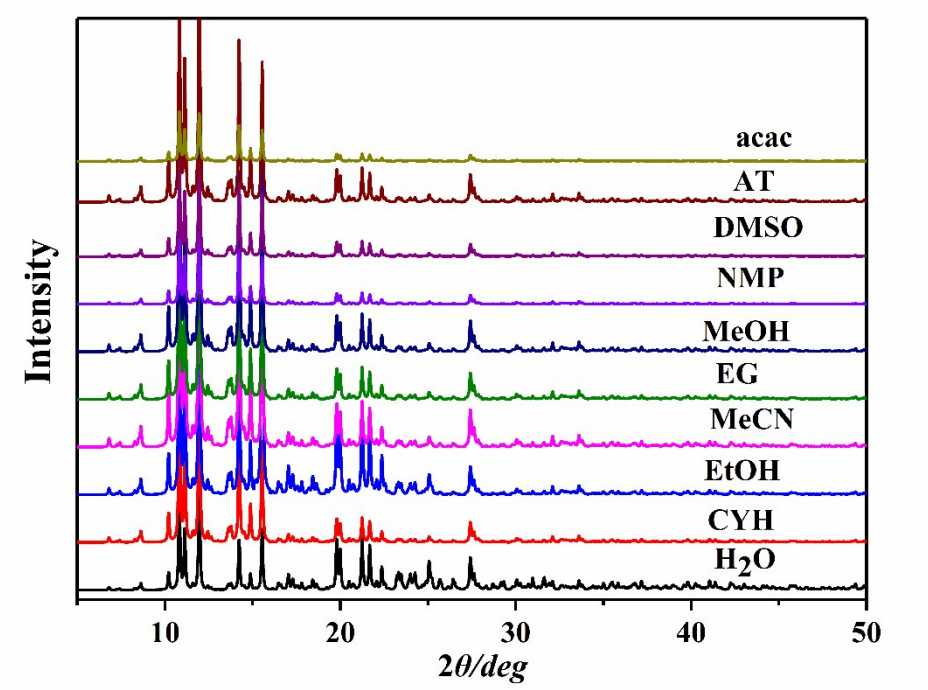

(a)

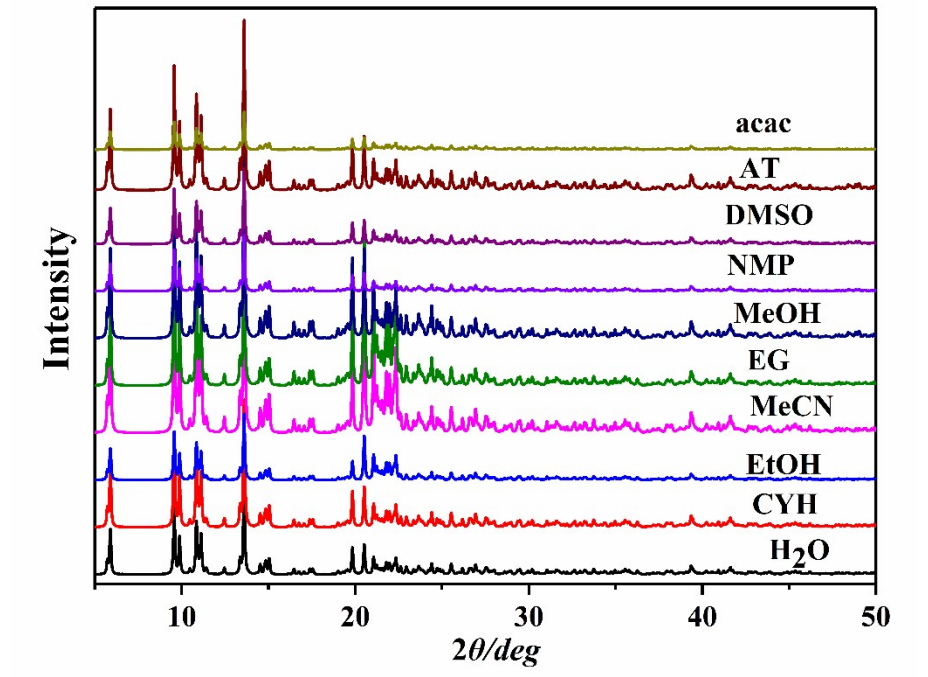

(b)

Fig. S12. The PXRD patterns of **2** (a) and **3** (b) were measured in different solvents.

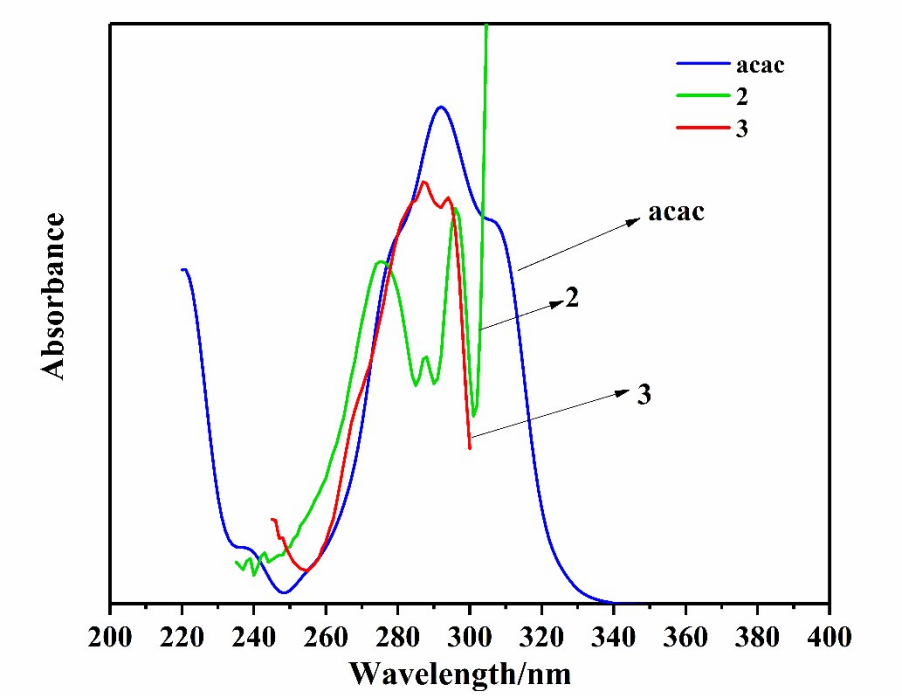

Fig. S13. Spectral overlap between the absorption spectra of acac ions and the excitation spectra of **2** and **3**.

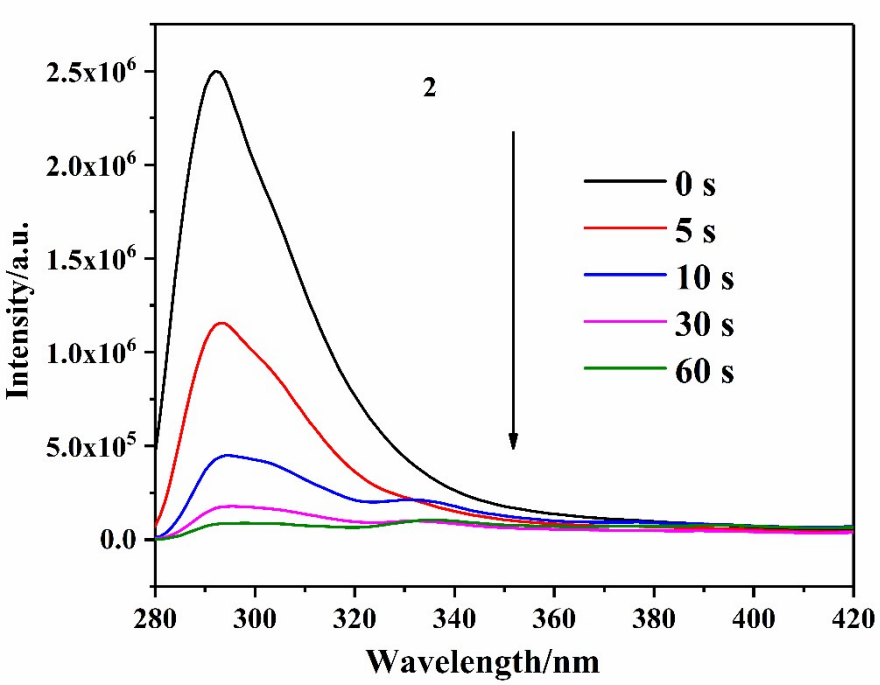

Fig. S14. In **2**, the time required for the quenching efficiency of Fe^{3+} ions to reach the maximum.

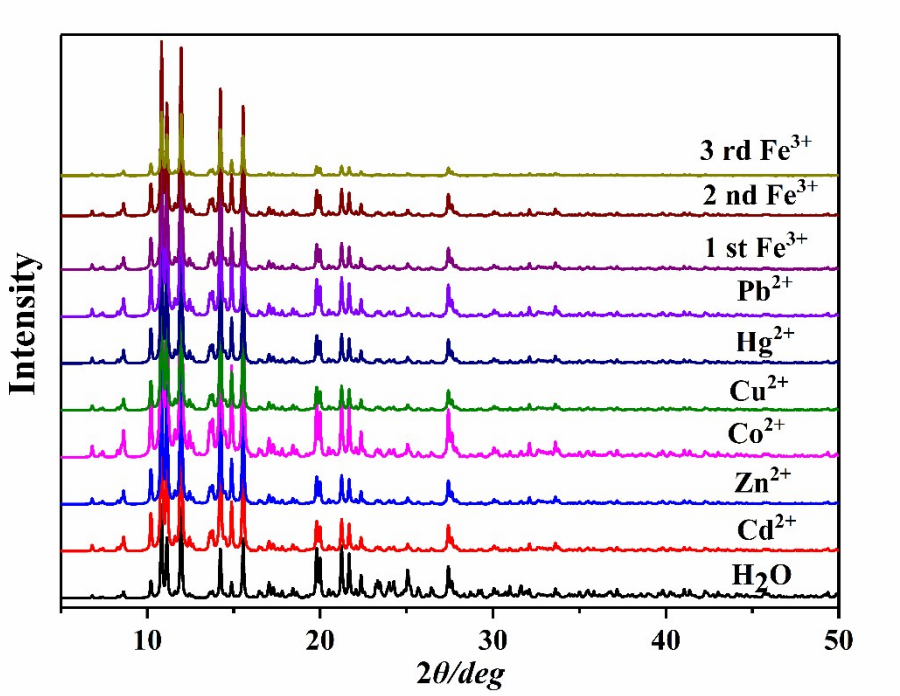

Fig. S15. PXRD patterns of **2** (samples were immersed in EtOH/H_2O solution containing Fe^{3+} ions and other common cations).

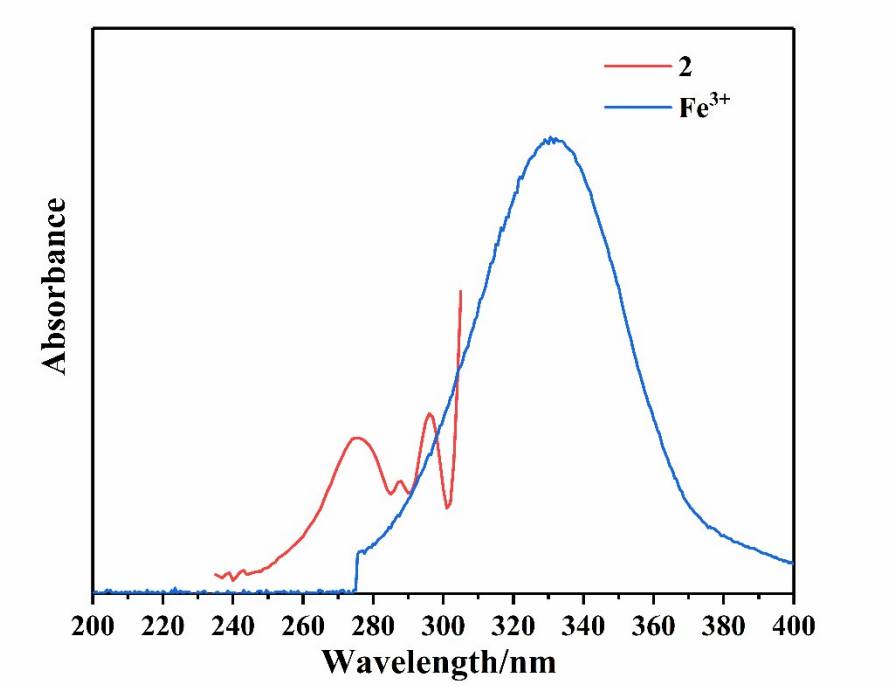

Fig. S16. Spectral overlap between the absorption spectra of Fe^{3+} ions and the excitation spectra of **2**.

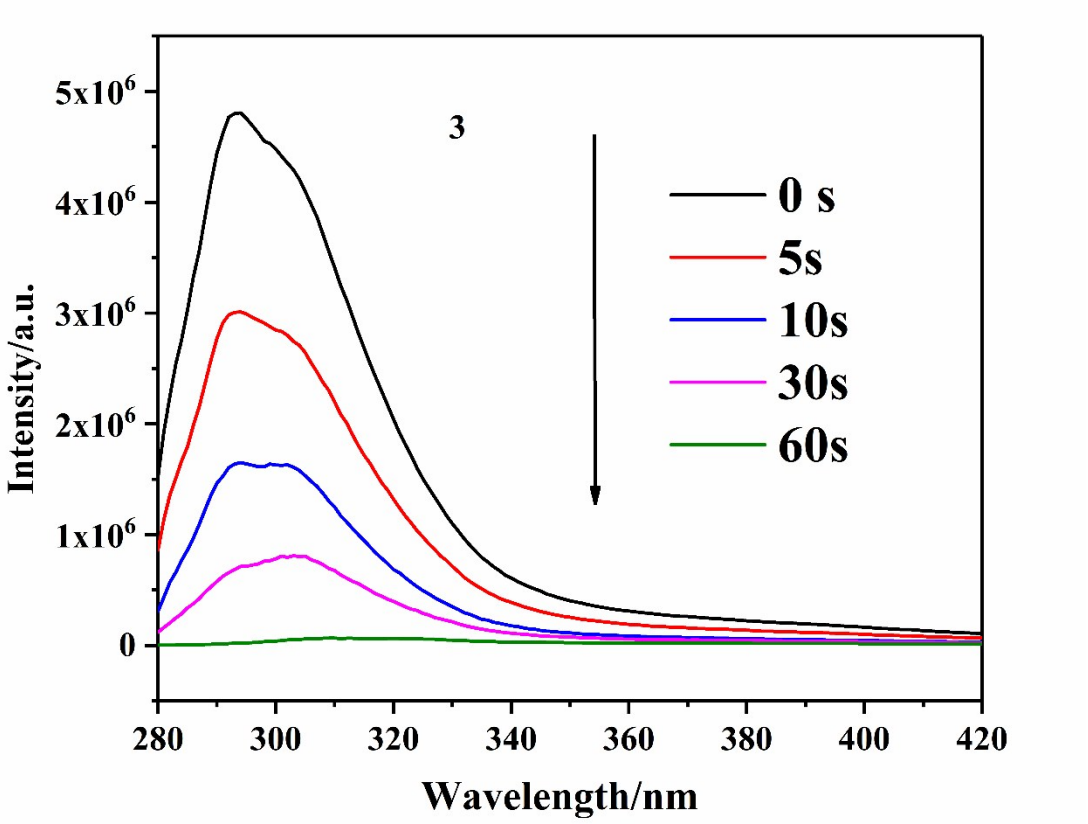

Fig. S17. In **3**, the time required for the quenching efficiency of $Cr_2O_7^{2-}$ anions to reach the maximum.

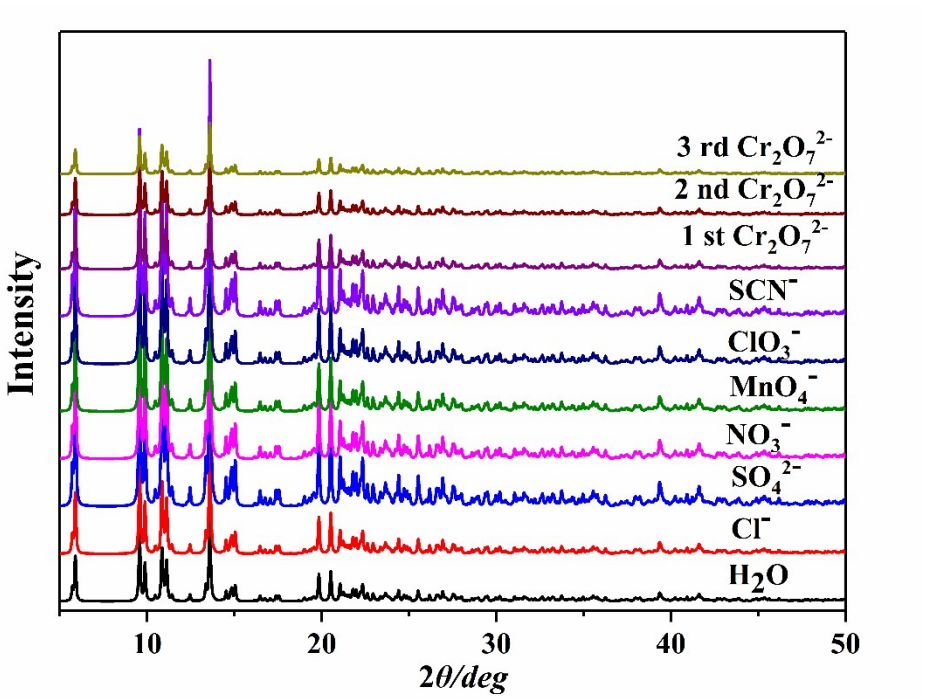

Fig. S18. The PXRD patterns of **3** sample was immersed in EtOH/H_2O solution containing $Cr_2O_7^{2-}$ anions and other common anions.

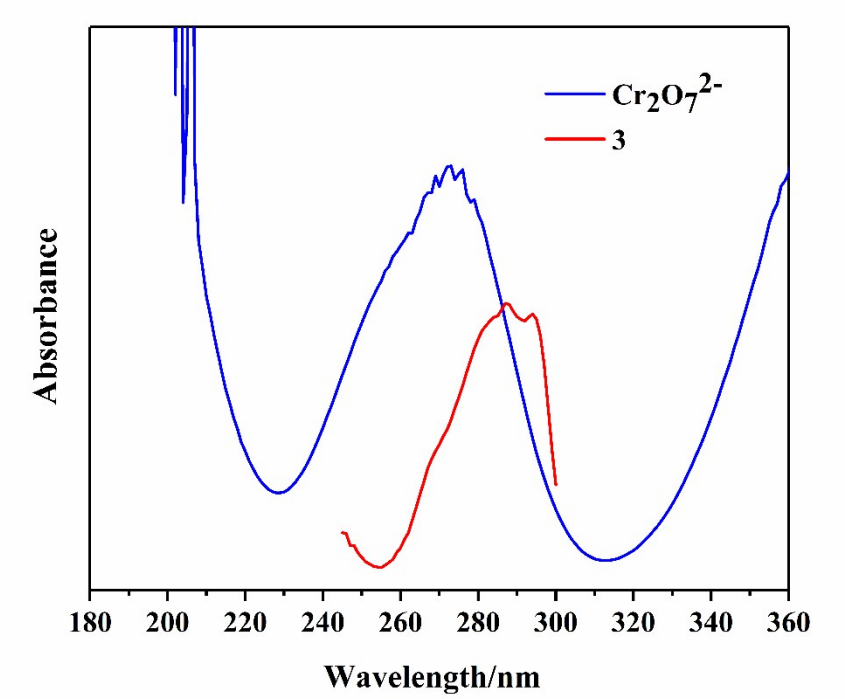

Fig. S19. Spectral overlap between the absorption spectra of $Cr_2O_7^{2-}$ anions and the excitation spectra of **3**.

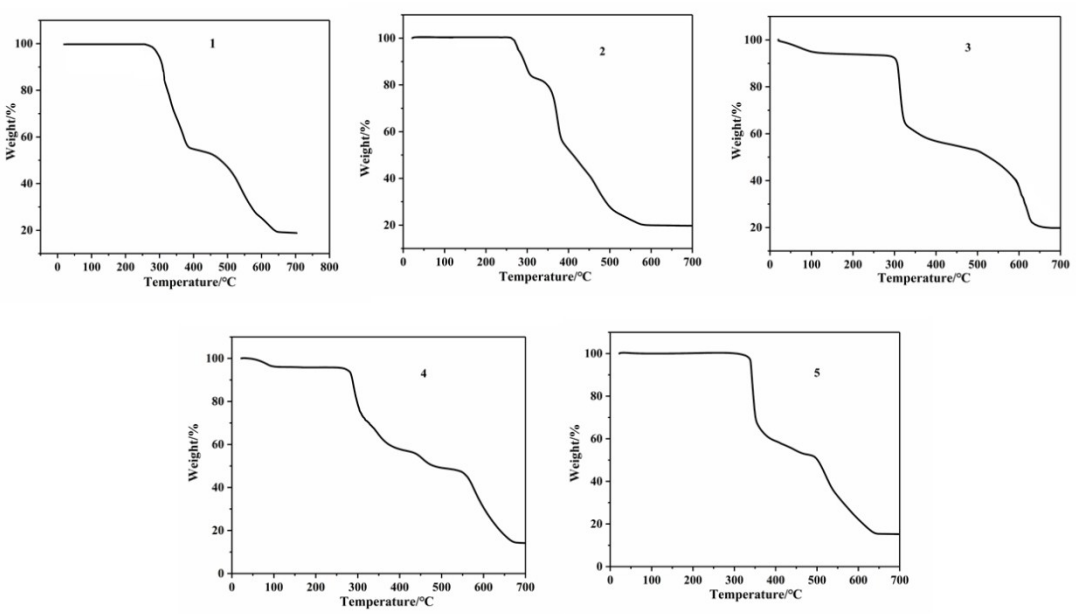

Fig. S20. TGA curves of Cd-MOFs **1**–**5.**

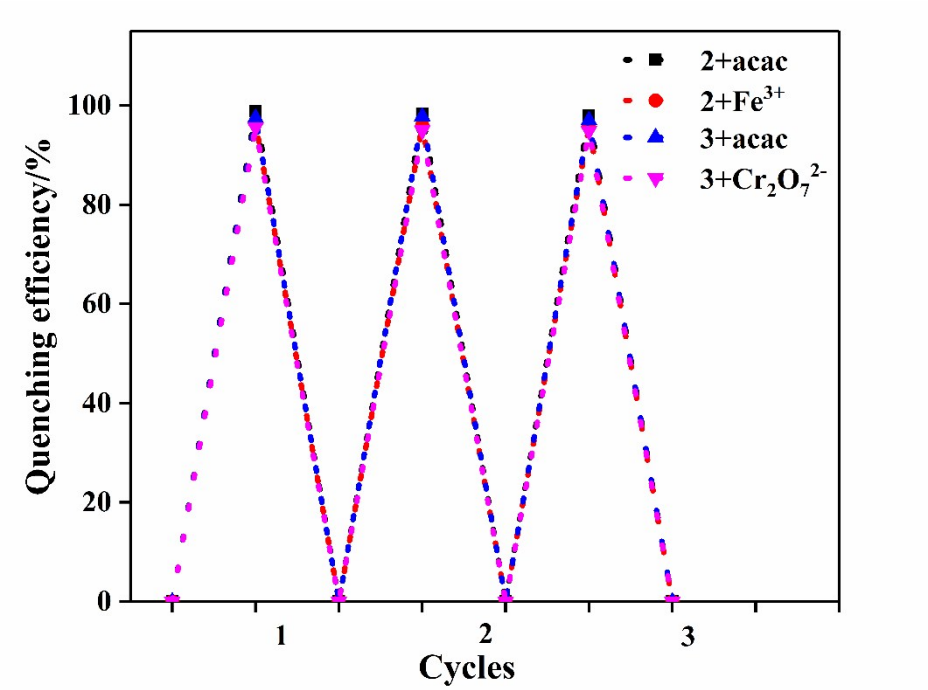

Fig. S21. Comparison of the quenching efficiency of **2** for sensing acac/Fe^{3+}, and **3** for acac/$Cr_2O_7^{2-}$ over three cycles.

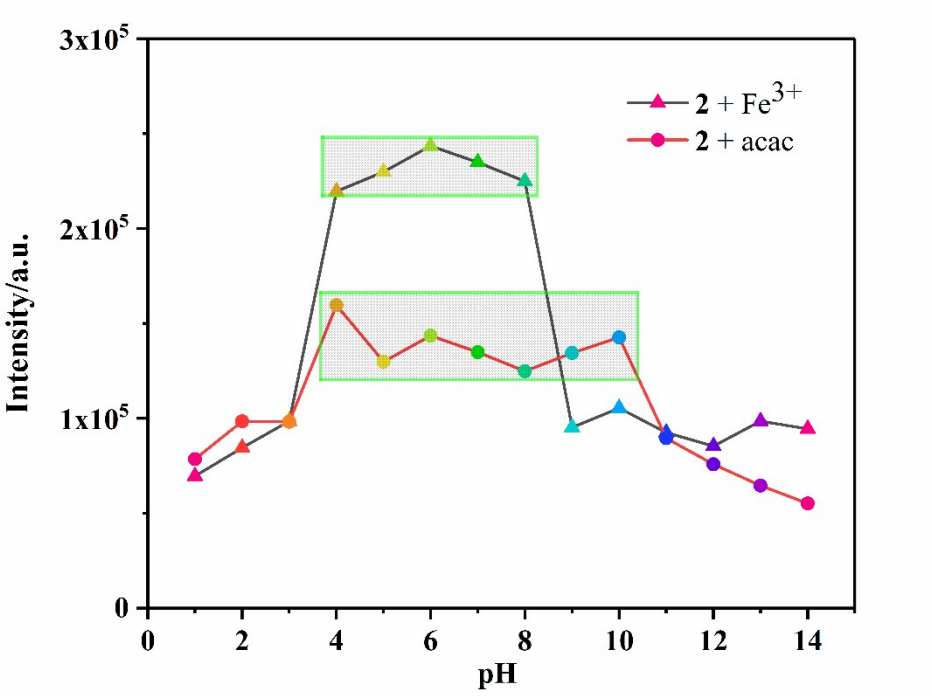

(a)

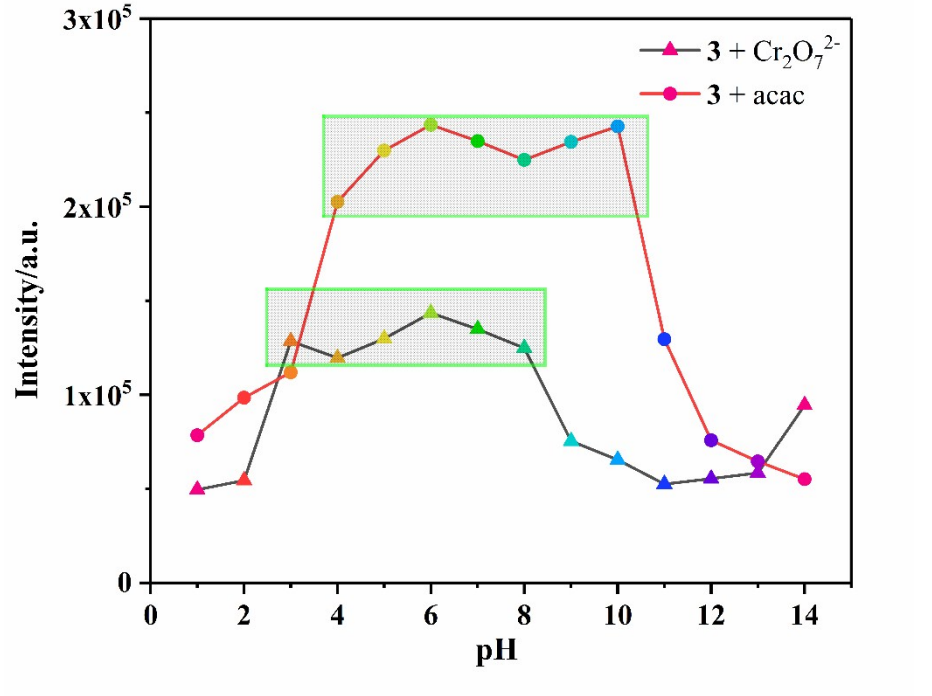

(b)

Fig. S22. (a) Effects of pH on the fluorescence maxima of **2** + acac (circle) and **2** + Fe^{3+} (triangle); (a) Effects of pH on the fluorescence maxima of **3** + acac (circle) and

3 + $Cr_2O_7^{2-}$ (triangle). Solvent: EtOH/H_2O (1:1, v/v).

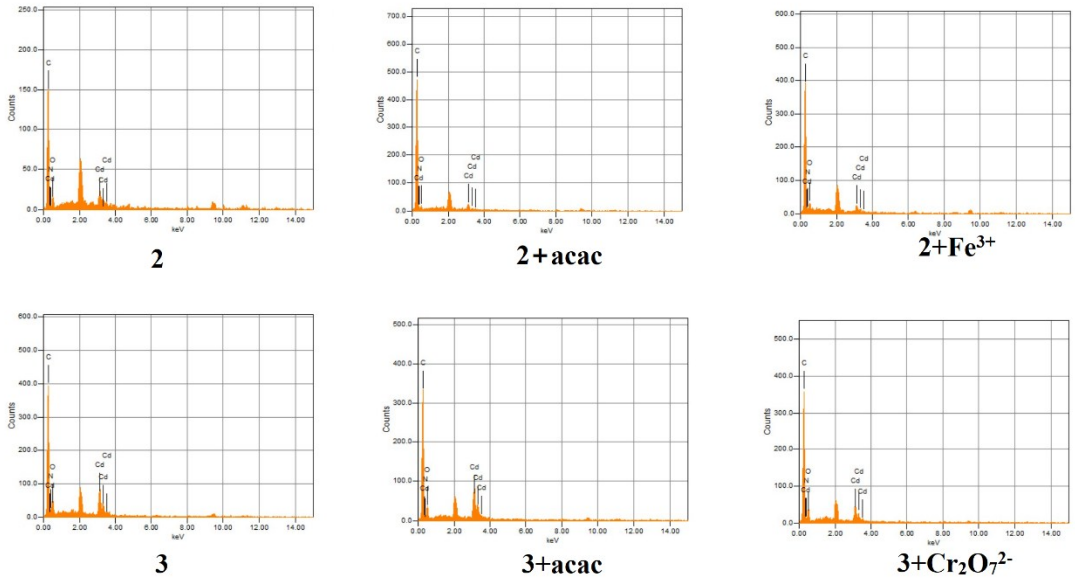

Fig. S23. The EDX patterns of **2** and **3**; **2** + acac, **3** + acac; **2** + Fe^{3+}, **3** + $Cr_2O_7^{2-}$, respectively.